Geochemical Perspectives Letters

Archean age and radiogenic source for the world's oldest emeralds

R.W. Nicklas[1*], J.M.D. Day[1], R. Alonso-Perez[2]

https://doi.org/10.7185/geochemlet.2232

Abstract

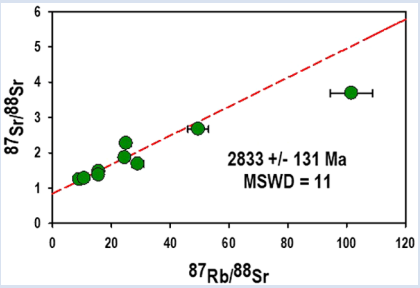

New ^{87}Rb-^{87}Sr data are reported for emeralds from Gravelotte, South Africa and Muzo, Colombia, the first such data in 30 years. The Gravelotte deposit is inferred to be the world's oldest emerald deposit from the ~2.97 Ga U-Pb age of the associated pegmatite. The majority of Gravelotte emeralds plot on an ^{87}Rb-^{87}Sr errorchron with an age of 2883 ± 131 Ma, close to the pegmatite age, demonstrating that the emeralds are Mesoarchean in age. The Muzo emerald data, when combined with data from nearby Colombian emerald deposits, define an age of ~48 Ma, younger than muscovite Ar-Ar ages (65–62 Ma), likely reflecting the resetting of ^{87}Rb-^{87}Sr in some emeralds. The initial Sr isotopic composition for Gravelotte emeralds is radiogenic (^{87}Sr/^{86}Sr$_i$ = 0.841), and their trace element signatures support their formation from a mature, high Rb/Sr, felsic continental crustal protolith in the Mesoarchean. Direct ^{87}Rb-^{87}Sr dating of emeralds holds promise for offering constraints on both mineralisation ages and source compositions.

Received 19 May 2022 | Accepted 25 August 2022 | Published 29 September 2022

Introduction

Emeralds are a variety of beryl ($Be_3Al_2Si_6O_{18}$) that are valued for their vibrant green colour, derived from the chromophore elements V, Cr and Fe. Emeralds are thought to form by the interaction of Be-enriched magmatic or aqueous fluids or hydrous evolved melts with V- and Cr-rich ultramafic or sedimentary country rocks (*e.g.*, Giuliani *et al.*, 2019). Emeralds are important gemstones for examining crustal processes because, compared to other gems, they contain high abundances of trace elements that can reveal their provenance (*e.g.*, Aurisicchio *et al.*, 2018; Giuliani *et al.*, 2019) and petrogenesis (Alonso-Perez and Day, 2021). Among trace elements, Rb and Sr can occur at concentrations >10 µg/g in bulk emeralds. Despite high concentrations of Rb and Sr, only a single study has utilised the commonly employed ^{87}Rb-^{87}Sr ($t_{1/2} = 4.72 \times 10^{10}$ yr^{-1}) isotope system to study emeralds (Vidal *et al.*, 1992), showing that old emeralds (~600 Ma) can host extremely radiogenic ^{87}Sr/^{86}Sr ratios (>65) due to the high ^{87}Rb/^{86}Sr ratios in some samples (up to ~11,000).

Reported ages for emerald deposits have dominantly been obtained from the ^{40}K-^{40}Ar or ^{40}Ar-^{39}Ar ages of coexisting micas (Cheilletz *et al.*, 1993; Svadlenak, 2015) (Fig. 1a), not of the emeralds themselves. Given the often polymetamorphic nature of emerald deposits, such ages may only represent the minimum age for emerald mineralisation. For the presumed oldest emerald deposit in the world, Gravelotte-Leydsdorp (henceforth Gravelotte), South Africa, the assumed age of ~2.97 Ga comes from indirect U-Pb zircon dating of associated rocks (Poujol, 2001; Lum *et al.*, 2016). Gravelotte emeralds have been shown to have geochemical signatures consistent with an S-type granite protolith (Alonso-Perez and Day, 2021). Their association with the Pan-African metamorphic belt and other emeralds with similar compositions in Zambia and Madagascar may indicate that they date to only ~900 to 600 Ma (Rino *et al.*, 2008). To determine if Gravelotte emeralds are indeed Archean in age, we report Rb-Sr isotope systematics and trace element abundances for them, as well as for the younger Muzo deposit in Colombia. An Archean age for Gravelotte emeralds would indicate that collisional tectonics and hydrothermal alteration of the continental crust was taking place at ~3 Ga.

Samples and Methods

Eight cut Gravelotte emeralds (GE-1 to GE-8) were analysed and all showed dark inclusions (Fig. 1c, Supplementary Information), likely biotite that is abundant in Gravelotte emeralds (Lum *et al.*, 2016). In addition, two samples from the same lot of uncut emeralds from the Muzo deposit, Colombia, were analysed (MGMH#97472-1 and MGMH#97472-2; Fig. 1b). Samples were digested using protocols outlined previously in Alonso Perez and Day (2021) at the Scripps Isotope Geochemistry Laboratory (SIGL, Scripps Institution of Oceanography). Digestions necessarily integrated the trace element and Rb-Sr isotopic signatures of the inclusions and their emerald lattices. A sample solution aliquot was analysed for major and trace element concentrations. Strontium separation chemistry was then performed using a two-step column chromatography procedure, after which purified Sr cuts were run on a *ThermoScientific Triton* thermal ionisation mass spectrometer at the SIGL. Details of the analytical methods and samples are provided in the Supplementary Information.

1. Scripps Institution of Oceanography, University of California San Diego, La Jolla, CA 92093, USA
2. Department of Earth and Planetary Sciences, Harvard University, Cambridge, MA 02138, USA
* Corresponding author (email: rnicklas@ucsd.edu)

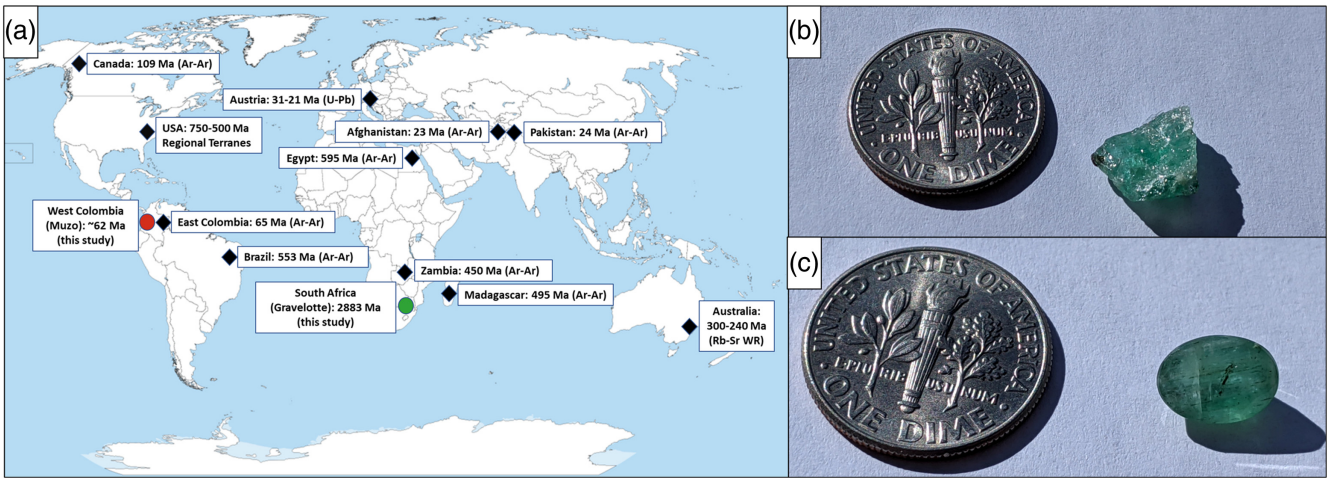

Figure 1 **(a)** Map of major dated emerald deposits, with the studied deposits highlighted in red (Muzo) and green (Gravelotte). Listed ages come from ^{87}Rb-^{87}Sr whole rock dating (Australia), U-Pb apatite dating (Austria), Ar-Ar mica dating (Afghanistan, Brazil, Canada, Colombia, Egypt, Madagascar, Pakistan and Zambia) or inferred from regional terrane ages (USA). Deposit ages are taken from Groat *et al.* (2002) and the compilations of Giuliani *et al.* (2019) and Alonso-Perez and Day (2021). **(b)** Muzo sample 97472-1, dime for scale. **(c)** Gravelotte sample GE-3, dime for scale.

Results

Major and trace element abundances and ^{87}Rb-^{87}Sr data are reported in Tables 1 and S-1 and the abundance data are consistent with those previously reported for their respective deposits (Alonso-Perez and Day, 2021) (Fig. 2). Gravelotte samples GE-1 through GE-5 have broadly similar REE patterns (normalised to continental crust, CC) with variable negative Ce anomalies, high La/Yb$_{CC}$ (1.9 ± 1.1) and low Ho/Yb$_{CC}$ (0.57 ± 0.19), consistent with their classification as Type IA emeralds (Alonso-Perez and Day, 2021). Emeralds GE-6 and GE-8 have flatter REE patterns with similar Ho/Yb$_{CC}$ (0.46 ± 0.14) but lower La/Yb$_{CC}$ (0.56 ± 0.12), and GE-7 is distinct in having elevated LREE/HREE (La/Yb$_{CC}$ = 22; Ho/Yb$_{CC}$ = 1). Samples GE-7 and GE-8 are heavily included, with dark fracture-filling material (Supplementary Information).

Gravelotte emeralds have ^{87}Rb/^{86}Sr and measured ^{87}Sr/^{86}Sr from 9.1 to 102 and from 1.25 to 8.16, respectively, more extreme than those for Muzo (^{87}Rb/^{86}Sr = 5.9–34.4, ^{87}Sr/^{86}Sr = 0.7213–0.7379). Notably, the Sr concentrations of the samples (0.08–3.87 µg/g) range to higher values than *in situ* data for global emeralds (0.02–0.11 µg/g; Aurisicchio *et al.*, 2018), indicating that a significant portion of the measured Sr was likely hosted in inclusions. Published *in situ* data for Colombian emeralds specifically (0.04–0.10 µg/g Sr; Aurisicchio *et al.*, 2018) are similarly lower than the new bulk Muzo data (0.14–0.16 µg/g Sr). Inclusion digestion likely also led to the lower Rb/Sr of the studied samples (2–28) compared to *in situ* Rb/Sr (13–6020; Aurisicchio *et al.*, 2018). The method employed here integrates the inclusions and emerald lattices and assumes that any inclusions are cogenetic with the emeralds.

Table 1 Rubidium-strontium isotope systematics of emeralds and replicate digestions of USGS standard reference material BHVO-2, with initial ^{87}Sr/^{86}Sr ratios for the Gravelotte samples at 700 Ma (Pan-African) and 2960 Ma (Deposit Age).

Sample	Rb (µg/g)	Sr (µg/g)	^{87}Rb/^{86}Sr	2 s.d.	^{87}Sr/^{86}Sr	2 s.e.	(^{87}Sr/^{86}Sr)$_{700\ Ma}$	(^{87}Sr/^{86}Sr)$_{2960\ Ma}$
GE-1	8.62	1.10	24.5	1.7	1.867963	0.000029	1.63	0.85
GE-2	1.99	0.26	25.0	1.8	2.272476	0.000066	2.03	1.23
GE-3a	8.19	0.87	29.0	2.0	1.685235	0.000016	1.41	0.48
GE-3b	11.8	3.87	9.07	0.6	1.249522	0.000020	1.16	0.87
GE-3c	14.1	2.73	15.6	1.1	1.473472	0.000048	1.32	0.82
GE-3d	12.0	2.32	15.6	1.1	1.373425	0.000014	1.22	0.73
GE-3e	12.8	3.56	10.7	0.8	1.281804	0.000010	1.18	0.84
GE-4	10.4	0.37	102	7.2	3.68916	0.00057	2.71	−0.54
GE-5	10.7	0.73	49.5	3.5	2.67065	0.00012	2.19	0.61
GE-6	0.52	0.08	30.1	2.1	8.1644	0.0071	7.87	6.91
GE-7	0.83	0.09	38.7	2.7	6.0647	0.0024	5.69	4.46
GE-8	4.69	0.39	49.7	3.5	5.27496	0.00056	4.80	3.21
97472-1	0.28	0.14	5.85	0.4	0.72131	0.00032		
97472-2	1.98	0.16	34.4	2.4	0.737875	0.000010		
BHVO-2	9.11	396	0.065	0.005	0.703456	0.000005		
BHVO-2	9.11	396	0.065	0.005	0.703453	0.000004		

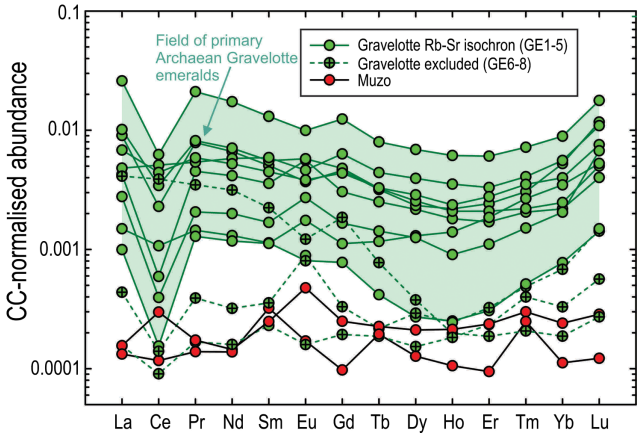

Figure 2 Sample REE abundance patterns normalised to continental crust (CC) (Rudnick and Gao, 2014).

Assuming similar origins for the Muzo and proximal Peñas Blancas deposits (Vidal *et al.*, 1992), these samples plot on an isochron (MSWD = 1.6) with an age of 48.7 ± 3.2 Ma and $^{87}Sr/^{86}Sr_i = 0.71724 \pm 0.00057$ (Fig. 3c). The Gravelotte data do not plot on a single isochron. Samples GE-1, GE-2, GE-3a–e, GE-4 and GE-5 show a positive correlation between $^{87}Rb/^{86}Sr$ and $^{87}Sr/^{86}Sr$, whereas GE-6, GE-7 and GE-8 show extremely radiogenic $^{87}Sr/^{86}Sr$ ratios (5.27–8.16) and only moderate $^{87}Rb/^{86}Sr$ (30–50), plotting away from the other samples. The spatial relationships between these three emeralds and the other samples within the deposit are unknown. Excluding the anomalous emeralds (GE-6–8) on the basis of their distinct low-Al contents and REE patterns yields an errochron (MSWD = 11) with an age of 2883 ± 131 Ma and $(^{87}Sr/^{86}Sr)_i = 0.841 \pm 0.031$ (Fig. 3b).

Discussion

Dating emeralds using Rb-Sr isotope systematics. Emeralds extend to high $^{87}Sr/^{86}Sr$ (>65; Vidal *et al.*, 1992) due to the greater affinity of Rb over Sr for beryl and the Precambrian ages of some samples, making the ^{87}Rb-^{87}Sr system useful for dating their mineralisation. The newly reported data facilitate the first direct dating of the Gravelotte emerald deposit and offers age constraints on the economically important Colombian Western Emerald Zone.

Gravelotte samples GE-6, GE-7 and GE-8 have radiogenic Sr contents that are unsupported by their $^{87}Rb/^{86}Sr$ values. On the 1/Sr *versus* $^{87}Sr/^{86}Sr$ plot (Fig. 3a), these samples have the lowest Sr contents and highest Sr isotopic compositions of the data set. These three samples also have low, non-stochiometric Al_2O_3 contents (4.7–7.4 wt. %), indicating that they likely contain significant fractions of low-Al fluid and mineral inclusions, and so may have been susceptible to resetting. For the three samples to have been displaced from the isochron, they must have lost 83 % (GE-6), 70 % (GE-7), and 54 % (GE-8) of their Rb or gained radiogenic Sr. Rubidium is likely hosted either in saline fluid inclusions or within the channels formed by the beryl structure (Groat *et al.*, 2008). Consequently, emerald Sr isotopic compositions may be susceptible to metamorphic disturbance. The non-coherence of GE-6, GE-7 and GE-8 indicates that analyses of closely associated crystals within a deposit will be beneficial in future studies. Such Rb-Sr isotopic disturbances may also be useful for examining metamorphic heating events affecting emeralds. In the case of Gravelotte, GE-6, GE-7 and GE-8 do not yield meaningful ages, but, assuming Rb loss rather than ^{87}Sr gain, their high measured $^{87}Sr/^{86}Sr$ values might

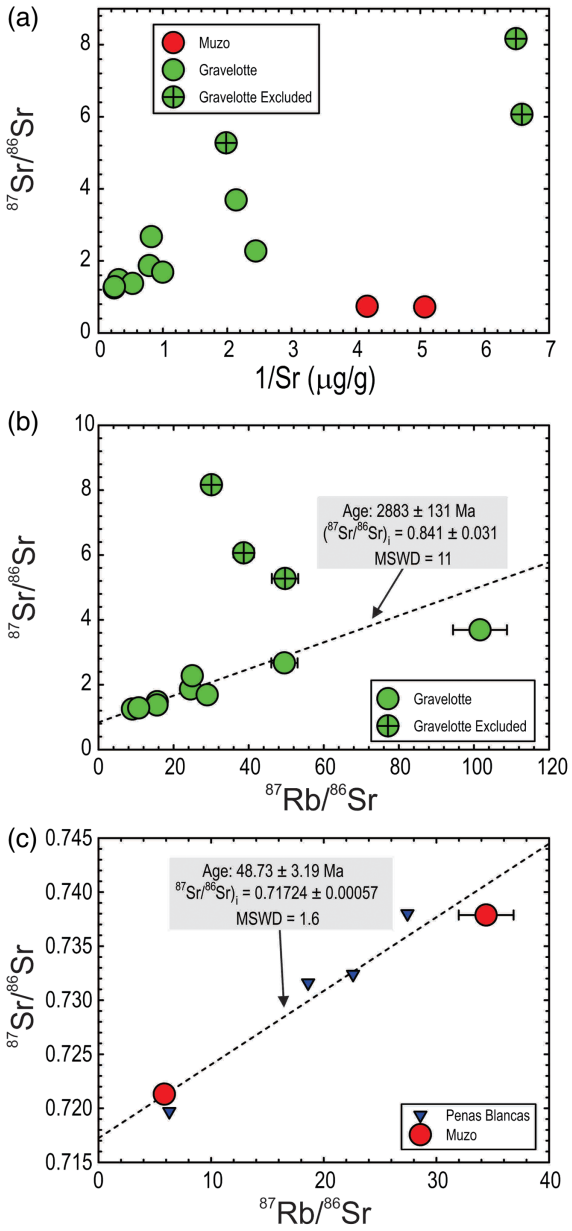

Figure 3 **(a)** Sample 1/Sr (in µg/g) plotted against $^{87}Sr/^{86}Sr_i$ ratios. Error bars shown for $^{87}Sr/^{86}Sr$ are 2 s.e. The three most radiogenic Gravelotte emeralds were likely reset and were excluded from the isochron ("Gravelotte excluded"; see main text for details). **(b)** $^{87}Rb/^{86}Sr$ plotted against $^{87}Sr/^{86}Sr$ for Gravelotte Emeralds. Error bars are 2 s.e. for the $^{87}Sr/^{86}Sr$ ratios and 7.07 % for $^{87}Rb/^{86}Sr$ ratios. The straight line is an errorchron (MSWD = 11) for the Gravelotte emeralds. **(c)** Rb-Sr data for Muzo (this study) and Peñas Blancas emeralds (Vidal *et al.*, 1992). The straight line is an isochron (MSWD = 1.8) for both datasets. All isochron calculations were performed using Isoplot 3.0 (Ludwig, 2003).

suggest relatively recent, rather than ancient, disturbances. These samples are excluded from further discussion of ages.

Archean Gravelotte emeralds. The remaining undisturbed Gravelotte samples yield a nine-point errorchron (MSWD = 11) with an age of 2883 ± 131 Ma and a radiogenic initial $^{87}Sr/^{86}Sr$ of 0.841 ± 0.031 (Fig. 3b). Although the high MSWD indicates additional uncertainty on the age, the measured initial $^{87}Sr/^{86}Sr$ of the samples lies within the permissible range of Archean continental crust (Table 1). The scatter of the data is likely due to $^{87}Sr/^{86}Sr$ heterogeneity at the time of deposit formation and possible

minor isotopic disequilibrium between Sr-rich inclusions and the emerald lattice during mineralisation. The errorchron age is within the uncertainties of the 2.969 Ga age of coexisting pegmatites (Poujol, 2001). This Archean ^{87}Rb-^{87}Sr age confirms that the Gravelotte deposit was formed in the Archean, and not by regional metamorphism during the Pan-African Orogeny ~900–600 Ma because the initial ^{87}Sr/^{86}Sr ratios are too radiogenic at 700 Ma (1.16–2.71) to be sourced from reasonable crustal protoliths. This age confirms that emerald formation, and corresponding extensive fractionation and alteration of the CC, was occurring in the Archean.

Rubidium-strontium isotopes in Colombian emeralds. Only two Muzo samples were measured, but Vidal *et al.* (1992) measured Rb-Sr isotopes in samples from the Peñas Blancas deposit, also in the Colombian Western Emerald Zone. The combined isochron (MSWD = 1.6) for both deposits yields an age of 48.7 ± 3.2 Ma with ^{87}Sr/^{86}Sr$_i$ = 0.71724 ± 0.00057 (Fig. 3c). This age is intermediate between the two groups of Muzo muscovite Ar-Ar ages at ~62 Ma and ~30 Ma (Svadlenak, 2015), and younger than the ^{87}Rb-^{87}Sr age of the Peñas Blancas deposit alone (~61 ± 5 Ma; Vidal *et al.*, 1992), suggesting the recent disturbance of the Muzo deposit but not the Peñas Blancas deposit. This is consistent with Muzo sample 97472-2 plotting to the right of the isochron (within the error envelope), indicating the possible late gain of Rb at ~30 Ma (Fig. 3c). There is a need for further Rb-Sr isotope dating of individual Colombian crystals and associated minerals, especially as it is currently unknown if Peñas Blancas and Muzo emeralds formed contemporaneously from isotopically similar fluids. Furthermore, the Eastern Emerald Zone deposits of Colombia have more coherent muscovite Ar-Ar ages (65–60 Ma; Svadlenak, 2015) and are therefore important targets for ^{87}Rb-^{87}Sr dating.

Using ^{87}Sr/^{86}Sr in emeralds to understand geological processes. Initial Sr isotopic compositions can reveal information on the sources of studied materials. In the case of the Gravelotte and Colombian Western Emerald Zone deposits, the age differences are matched by differences in ^{87}Sr/^{86}Sr$_i$. For the Colombian emeralds, the initial ^{87}Sr/^{86}Sr of 0.71724 is more radiogenic than typical Andean Northern Volcanic Zone lavas (~0.7045; *e.g.*, Errazuriz-Henao *et al.*, 2019), but falls within the range of Colombian plutonic rocks (0.7165–0.778; McCourt *et al.*, 1984). The fluids that formed the Western Emerald Zone deposit were therefore likely sourced from the local CC, consistent with previous conclusions (Ottaway *et al.*, 1994). The Muzo CC-like REE patterns and initial Sr isotope compositions therefore support the ultimate derivation of those sediments from uplifted and eroded basement rocks.

In contrast with Colombian emeralds, the South African Gravelotte emeralds are characterised by high ^{87}Sr/^{86}Sr$_i$ of ~0.841 ± 0.031, more radiogenic than the average values of 3 Ga CC, which only range up to ~0.73 (Goldstein, 1988). The ^{87}Sr/^{86}Sr$_i$ values of gneisses and plutons from the Barberton Greenstone belt, also in the Kaapvaal Craton but unrelated to Gravelotte, range from 0.7011 (3.35 Ga Barberton granodiorites) to 0.88 in younger (2.24 ± 0.36 Ga) Kaapvaal Craton Nhlangano gneisses (Barton *et al.*, 1983). Critically, some of the older plutons have high Rb/Sr (>10). These comparisons indicate that Gravelotte ^{87}Sr/^{86}Sr$_i$ values are not unreasonable. Such conclusions await data on cogenetic rocks from Gravelotte. Both the likely presence of highly differentiated lithologies at Gravelotte at 3 Ga and the inferred presence of pre-existing ancient high-Rb/Sr material supports the formation of mature CC-like rocks by the Mesoarchean at the latest.

It has previously been shown that Gravelotte emeralds show an upturned HREE pattern diagnostic of emeralds from Type IA deposits, *e.g.*, those associated with sediment melting during continent-continent collision (Alonso-Perez and Day, 2021). Our results for the Gravelotte emeralds confirm an Archean heritage, supporting the melting of S-type protoliths in the Mesoarchean and the concept that emerald geochemistry is useful for understanding collisional tectonics and plate tectonic processes (Alonso-Perez and Day, 2021).

In conclusion, new Rb-Sr isotope data show that Gravelotte is the oldest known emerald deposit and indicates that pegmatite formation was occurring at ~3 Ga. Fluid inclusion-rich, high-Rb/Sr emeralds lost significant Rb in a later thermal metamorphic event after the in-growth of significant quantities of ^{87}Sr. This conclusion awaits further work on the diffusion of Sr and Rb in the beryl structure. Future Sr isotope studies, either *in situ* or of bulk emeralds isolated from their inclusions, are a necessary step in proliferating the use of the Rb-Sr isotope system in understanding beryl genesis. Given the ability of the Rb-Sr isotope system to directly date emerald mineralisation, more global deposits should be targeted. The Archean age and radiogenic ^{87}Sr/^{86}Sr$_i$ value of the Gravelotte deposit suggests that emerald deposits in Precambrian terranes may be underexplored.

Acknowledgements

Financial support for this work came from the Scripps Institution of Oceanography and the Mineralogical and Geological Museum, Harvard University (MGMH). We are grateful to S. and A. Pouroulis for their generous provision of samples and excellent knowledge of the Gravelotte deposit. This work was improved by comments from reviewers Elis Hoffmann and Rainer Thomas, editor Horst Marschall and the earlier comments of David Chew.

Editor: Horst R. Marschall

Additional Information

Supplementary Information accompanies this letter at https://www.geochemicalperspectivesletters.org/article2232.

Cite this letter as: Nicklas, R.W., Day, J.M.D, Alonso-Perez, R. (2022) Archean age and radiogenic source for the world's oldest emeralds. *Geochem. Persp. Let.* 23, 23–27. https://doi.org/10.7185/geochemlet.2232

References

Alonso-Perez, R., Day, J.M.D. (2021) Rare earth element and incompatible trace element abundances in emeralds reveal their formation environments. *Minerals* 11, 513, 1–21. https://doi.org/10.3390/min11050513

Aurisicchio, C., Conte, A.M., Medeghini, L., Ottolini, L., De Vito, C. (2018) Major and trace element geochemistry of emerald from several deposits: Implications for genetic models and classification schemes. *Ore Geology Reviews* 94, 351–366. https://doi.org/10.1016/j.oregeorev.2018.02.001

Barton Jr., J.M., Hunter, D.R., Jackson, M.P.A., Wilson, A.C. (1983) Geochronologic and Sr-isotopic studies of certain units in the Barberton granite-greenstone terrane, Swaziland. *South African Journal of Geology* 86, 71–80.

Cheilletz, A., Feraud, G., Giuliani, G., Ruffet, G. (1993) Emerald dating through $^{40}Ar/^{39}Ar$ step-heating and laser spot analysis of syngenetic phlogopite. *Earth and Planetary Science Letters* 120, 473–485. https://doi.org/10.1016/0012-821X(93)90258-B

Errazuriz-Henao, C., Gomez-Tuena, A., Duque-Trujillo, J., Weber, M. (2019) The role of subducted sediments in the formation of intermediate mantle-derived magmas from the Northern Colombian Andes. *Lithos*, 336–337, 151–168. https://doi.org/10.1016/j.lithos.2019.04.007

Goldstein, S.L. (1988) Decoupled evolution of Nd and Sr isotopes in the continental crust and the mantle. *Nature* 336, 733–738. https://doi.org/10.1038/336733a0

Groat, L.A., Marshall, D.D., Giuliani, G., Murphy, D.C., Piercey, S.J., Jambor, J.L., Mortensen, J.K., Ercit, T.S., Gault, R.A., Mattey, D.P., Schwarz, D., Maluski, H., Wise, M.A., Wengzynowski, W., Eaton, D.W. (2002) Mineralogical and geochemical study of the regal ridge emerald showing, southeastern Yukon. *Canadian Mineralogist* 40, 1313–1338. https://doi.org/10.2113/gscanmin.40.5.1313

Groat, L.A., Giuliani, G., Marshall, D.D., Turner, D. (2008) Emerald deposits and occurrences: A review. *Ore Geology Reviews* 34, 87–112. https://doi.org/10.1016/j.oregeorev.2007.09.003

Giuliani, G., France-Lanord, C., Cheilletz, A., Coget, P., Branquet, Y., Laumomnier, B. (2000) Sulfate Reduction by Organic Matter in Colombian Emerald Deposits: Chemical and Stable Isotope (C, O, H) Evidence. *Economic Geology* 95, 1129–1153. https://doi.org/10.2113/gsecongeo.95.5.1129

Giuliani, G., Groat, L.A., Marshall, D., Fallick, A.E., Branquet, Y. (2019) Emerald Deposits: A Review and Enhanced Classification. *Minerals*, 105, 1–63. https://doi.org/10.3390/min9020105

Ludwig, K.R. (2003) ISOPLOT 3.00: A geochronological toolkit for Microsoft Excel. *Berkeley Geochronology Center Special Publication* 4, 1–70.

Lum, J.E., Viljoen, K.S., Cairncross, B. (2016) Mineralogical and geochemical characteristics of emeralds from the Leydsdorp area, South Africa. *South African Journal of Geology* 119, 2, 359–378. https://doi.org/10.2113/gssajg.119.2.359

McCourt, W.J., Aspden, J.A., Brook, M. (1984) New geological and geochronological data from the Colombian Andes: continental growth by multiple accretion. *Journal of the Geological Society* 141, 831–845. https://doi.org/10.1144/gsjgs.141.5.0831

Ottaway, T.L., Wicks, F.J., Bryndzia, L.T., Kyser, T.K., Spooner E.T.C. (1994) Formation of the Muzo hydrothermal emerald deposit in Colombia. *Nature* 369, 552–554. https://doi.org/10.1038/369552a0

Poujol, M. (2001) U-Pb isotopic evidence for episodic granitoid emplacement in the Murchison greenstone belt, South Africa. *Journal of African Earth Sciences* 33, 155–163. https://doi.org/10.1016/S0899-5362(01)90096-X

Rino, S., Kon, Y., Sato, W., Maruyama, S., Santosh, M., Zhao, D. (2008) The Grenvillian and Pan-African orogens: World's largest orogenies through geologic time, and their implications on the origin of superplume. *Gondwana Research* 14, 51–72. https://doi.org/10.1016/j.gr.2008.01.001

Rudnick, R.L., Gao, S. (2014) 4.1 - Composition of the Continental Crust. In: Holland, H.D., Turkenian, K.K. (Eds.) *Treatise on Geochemistry*. 2nd edition, Elsevier, Amsterdam, 1–51. https://doi.org/10.1016/B978-0-08-095975-7.00301-6

Svadlenak, E. (2015) $^{40}Ar/^{39}Ar$ Ages and Trace Element Variations in Colombian Emeralds. [Honors Baccalaureate Thesis], Corvallis, Oregon State University.

Vidal, Ph., Lasnier, B., Poirot, J.-P. (1992) Determination of the age and origin of emeralds using rubidium-strontium analysis. *Journal of Gemmology* 23, 198–200. https://doi.org/10.15506/JoG.1992.23.4.198

Geochemical Perspectives Letters

Archean age and radiogenic source for the world's oldest emeralds

R.W. Nicklas, J.M.D. Day, R. Alonso-Perez

Supplementary Information

The Supplementary Information includes:

- Supplementary Text
- Table S-1
- Figures S-1 to S-6
- Supplementary Information References

Supplementary Text

Sample Background

The Gravelotte-Leydsdorp (henceforth Gravelotte) emerald deposit of South Africa is presumed to be the oldest identified occurrence of emeralds on Earth, based on indirect dating to the early Neoarchaean at ~2.97 Ga (Robb and Robb, 1986; Poujol, 2001; Lum *et al.*, 2016). The age of the deposit is close to that of the oldest known occurrence of any type of beryl at ~3 Ga (Grew and Hazen, 2014). According to the recent classification system of (Giuliani *et al.*, 2019), the Gravelotte deposit is Type IA, formed by the interaction of Be-rich pegmatitic fluids with ultramafic rocks. Alonso-Perez and Day (2021) argued based on emerald trace element geochemistry that Type IA Gravelotte emeralds formed from magmatic fluids of sedimentary (S)-type granitic melts interacting with Cr, V-rich mafic–ultramafic crustal protoliths. Although it has been recognised that emeralds may also be formed by hydrous silicate melts and not just aqueous fluids (Thomas *et al.*, 2020), all available inclusion data indicate that the Gravelotte deposit formed by aqueous fluid circulation (Nwe and Morteani, 1993). These ultramafic schists are likely the source of Cr and V and led to the stabilisation of deep-green emerald in veins within the schist (Robb and Robb, 1986; Grundmann and Morteani, 1989). The paragenetic association in the veins is emerald, phenakite, molybdenite, chalcopyrite, scheelite and native bismuth, indicating that the parental fluids were sulfur rich (Grundmann and Morteani, 1989).

At around 600 Ma, during the Pan-African Orogeny, the assemblage experienced greenschist-facies regional metamorphism (Grundmann and Morteani, 1989). The Gravelotte emeralds are notable among worldwide deposits for their high Cr and low V contents as well as their high abundance of biotite and fluid

inclusions (Lum *et al.*, 2016). The main chromophore in the Gravelotte emeralds is Cr and not V or Fe. Perhaps the most readily distinguishable chemical feature of Gravelotte emeralds is their uniquely high Na contents, ranging up to 2.3 wt. % Na_2O (Lum *et al.*, 2016). Notably, the age of the deposit is from a U-Pb zircon age of the pegmatite to be ~2.969 ± 0.014 Ga (Robb and Robb, 1986; Poujol, 2001) and no direct date for the mineralisation has been produced up to this point. Given the complications of later regional metamorphism affecting the deposit, the emeralds could reasonably be Pan-African (~600 Ma) in age. It is therefore important to constrain the age of the emeralds relative to their host rocks.

Eight cut gemstones Gravelotte emeralds provided by previous owners of the mine (Artemis and Salome Pourolis) labeled GE-1 through GE-8 and ranging in weight from 0.13 to 1.14 grams were using in this study. The emeralds, pictured in **Figure S-1**, are green, cloudy and show dark inclusions, likely biotite which is abundant in Gravelotte emeralds (Lum *et al.*, 2016) and is consistent with assemblages in emeralds (Saeseaw *et al.*, 2019). The cloudy nature of the emeralds is probably due to abundant fluid inclusions (Nwe and Morteani 1993; Lum *et al.*, 2016). The largest crystal, GE-3, was broken using a pre-cleaned ceramic mortar and pestle into fragments which were separated into five groups of approximately equal masses, labeled GE-3a through GE-3e. These five fragmentary samples are useful for examination of Rb-Sr isotope variability within a single crystal.

Colombian emerald deposits are found on both sides of the Cordillera Oriental, the easternmost branch of the Andes in Colombia. The Muzo deposit lies in the Western Emerald Zone. Unlike most other emerald deposits, Colombian emeralds are hosted in veins within organic carbon rich black shale material, and ultramafic rocks are notably absent (Ottaway *et al.*, 1984). The Muzo deposit shows no evidence for magmatic activity and was likely formed by fluids released by regional metamorphism associated with the folding of the crust to build the Cordillera Oriental (Giuliani *et al.*, 2000; Groat *et al.*, 2008). Similar to the Gravelotte deposit, published inclusion geochemistry show that the Muzo deposit likely formed from an aqueous fluid not a silicate melt (Ottaway *et al.*, 1984). The Muzo mineralisation has been ^{40}Ar-^{39}Ar dated using hydrothermal muscovite in the veins to have been formed in two pulses between 62-60 Ma and 32-30 Ma (Svadlenak, 2015), the first pulse being similar to the ~60-65 Ma ^{40}Ar-^{39}Ar age for deposits from the Eastern Emerald Zone (Cheilletz *et al.*, 1993). Colombian emeralds from the Peñas Blancas deposit of the Western Emerald Zone have been previously analysed for Sr isotopic systematics, with $^{87}Sr/^{86}Sr$ ratios ranging between 0.7197 and 0.7380, and a Rb-Sr isochron age of ~62 Ma (Vidal *et al.*, 1992). Two samples of uncut emeralds from the Muzo deposit from the Mineralogical and Geological Museum, Harvard University (MGMH), were obtained for this study. Samples were numbered MGMH#97472-1 (0.44493 g) and MGMH#97472-2 (0.16428 g) and the second sample consisted of two small fragments (**Figure S-1**). Both samples show fewer inclusions and greater clarity than the Gravelotte samples.

Analytical Methods

The samples, ranging in weight between 0.109 and 0.445 g, were loaded uncrushed into screw-top Teflon vials along with a 4:1 ratio of distilled 27 M HF-15.7 M HNO_3 and were digested on the hotplate at 150 ºC for 72 hours. Standard reference material powders BHVO-2, BCR-2 and BIR-1 were also prepared, spanning a range of masses (~0.1–0.4 g) and treated in an identical manner to the samples. The dried residues of the initial digestion were then refluxed three times in 15.7 M HNO_3 on the hotplate to break down fluorides.

Sample solutions were prepared gravimetrically, and a 5 % aliquot was taken for major- and trace-element abundance determination. This aliquot was separated into two batches with an In tracer solution added to monitor sensitivity and instrumental drift. The first solution, for major and minor element abundances was

prepared with a dilution factor of 5000. A second solution was prepared for low abundance trace elements, including the rare earth elements, Rb and Sr, with a dilution factor of 1000. Major and trace element analyses were performed using a *ThermoScientific iCAP Qc* inductively coupled plasma mass spectrometer (ICP-MS) at the *Scripps Isotope Geochemistry Laboratory* (*SIGL*), *University of California, San Diego* using identical methods to those applied in Alonso-Perez and Day (2021). Data were compared to replicate digestions of the USGS standard reference material (SRM) BHVO-2. Precision of major and trace element concentrations are <5 %, as determined by digestions of a range of USGS SRMs (BIR-1, BCR-2, BHVO-2). Uncertainty on reported $^{87}Rb/^{86}Sr$ ratios is estimated at 7.07 %, propagated from 5 % uncertainties on Rb and Sr concentrations. Concentrations of SiO_2 were determined by difference of the sum of major oxides and 100 %, as silica is volatilised out of solution as SiF_6 during the initial HF digestion step. Water contents of the emeralds were estimated using the method of Giuliani *et al.*, (1997), where H_2O (in wt. %) = [0.84958 Na_2O (in wt. %)] + 0.8373.

Strontium separation chemistry followed a two-step column chromatography procedure using the *Biorad® AG50X8 200-400* resin and the *Eichrom® Sr-Spec* resin. After removing the 5 % aliquot for trace element analysis, the residual solutions were dried down and taken up in 10 N HCl, equilibrated and then dried down. The sample residues were then taken up in 1.5 M HCl until a clear solution was obtained. A series of calibrations were performed using SRM materials and emerald solutions to examine the behaviour of Rb, Sr and particularly Be on the columns before the valuable samples were introduced. The first stage chemistry served to remove Be and most trace elements from the solution. First the sample solution was loaded on the pre-cleaned 1.8 mL resin bed in 2 mL of 1.5 M HCl. The bulk of the matrix elements along with Pb and Hf were washed off the column with 12 further mL of 1.5 M HCl. The REE and Sr were then eluted using 12 mL of 6 M HCl. The second stage column served to isolate Sr from Al and remaining trace elements, especially Rb, although the high Rb/Sr meant some solutions after this step still had minor quantities of Rb. The REE-Sr solution was loaded onto the pre-cleaned resin in 1 mL 4 M HNO_3. The REE and remaining matrix elements were eluted in 10 mL of 4 M HNO_3 and then Sr was eluted in 10 mL of warm H_2O. The final Sr cuts were evaporated to dryness before being loaded on degassed rhenium filaments along with a TaF_5 activator solution for analysis by Thermal Ionization Mass Spectrometry (TIMS). After loading and drying, the filaments were glowed in air for ~30 seconds to burn off excess Rb to reduce the in-run ^{87}Rb interference correction. The filaments were run on a *ThermoScientific Triton* TIMS at the *SIGL* and corrected for instrumental mass fractionation using $^{86}Sr/^{88}Sr = 0.1194$. Filaments were run between 1411 and 1657 ºC for 360 ratio measurements or until the ^{88}Sr signal faded below 10^{-3} volts. Three samples (GE-6, GE-5 and 97472-1) faded after 80, 184 and 220 ratios respectively and show correspondingly high uncertainties, but all other samples lasted a full 360 ratios. Repeated analyses of the NBS987 standard reference material yielded an average $^{87}Sr/^{86}Sr$ ratio of 0.710231 ± 0.000015 (2SE, n = 5). Replicate digestions of the USGS standard reference material BHVO-2 prepared with the samples (**Table S-1**) had an average $^{87}Sr/^{86}Sr$ ratio of 0.703455 ± 0.000002 (2SE, n = 2), within uncertainty of the GEOREM preferred ratio of 0.703478 ± 0.000034. The $^{87}Sr/^{86}Sr$ ratios were corrected for interference from ^{87}Rb by measurement of the ^{85}Rb peak, and all the reported runs showed average in-run $^{85}Rb/^{88}Sr < 0.0616$. An examination of the relative effects of ^{87}Rb interference on the reported data can be found in **Figure S-2** and this interference was found to be negligible for the sample runs. The relative difficulty of removing Rb from high Rb/Sr materials such as beryls has perhaps contributed to the limited quantity of Sr isotopic data available for emeralds.

Supplementary Discussion

A notable feature of the REE patterns is the negative (<1) Ce anomaly ($Ce/Ce^* = Ce_N/(La_N \times Pr_N)^{0.5}$) present in ten of the twelve Gravelotte emeralds, with Ce/Ce* in the Gravelotte emeralds ranging from 0.14 to 1.03 **(Figure 2, Figure S-3**). This contrasts with the Muzo emeralds which have Ce anomalies of 1.81 and 0.86. Cerium is unique among the REE in its tendency to form tetravalent species in highly oxidised environments, with such a species showing a much lower solubility in aqueous fluids than the neighbouring trivalent La and Pr (Byrne and Sholkovitz, 1996). The negative cerium anomalies may be a feature of the parental fluids to the Gravelotte emeralds, as Ce is less efficiently leached from igneous materials than the other REE. The parental fluids to the Muzo emeralds may have been more reduced than those of the Gravelotte emeralds, as suggested by Banks *et al.* (2000) based on fluid inclusion Fe/Mn ratios. They do not show such strongly negative Ce anomalies, consistent with low oxygen fugacity leading to insignificant Ce^{+4} formation. Previous work on fluid inclusions in Gravelotte emeralds (Nwe and Morteani, 1993) suggested the parental fluids were highly reducing at ΔFMQ = -2 but subsequently evolved to more oxidising values of ΔFMQ = +1, still not oxidising enough to stabilise significant Ce^{+4}. In contrast, Muzo parental fluids likely began highly reduced, in the graphite stability field, but oxidised ~4 log units by precipitation of reduced Fe in pyrite before precipitating emerald. It is also notable that the Gravelotte emeralds formed prior to the Great Oxidation Event (GOE) when the surface environment was anoxic (Lyons *et al.*, 2014) yet show oxidised signatures indicating that their parental fluids did not equilibrate significantly with the atmosphere. Muzo emeralds, despite forming during a period with abundant atmospheric oxygen, have reducing parental fluids, and therefore also did not interact with the atmosphere.

Negative Ce/Ce* anomalies such as those seen in Gravelotte are relatively rare among worldwide emerald deposits, although this may be an artifact of the limited data currently available for REE concentrations in emeralds. Currently there are not enough crystal chemistry constraints on the partitioning of REE into beryl nor enough constraints on the Ce/Ce* values of protoliths of the deposits to determine if Ce/Ce* in emerald is a useful tracer of parental fluid oxygen fugacity, but this appears to be a promising area of future research. Although the REE patterns of the two sites overlap, the Muzo emeralds show systematically lower CC-normalised $(La/Sm)_N$ than the Gravelotte emeralds (**Figure S-3**). Such a dichotomy is consistent with the origin of the parental fluids of Muzo emeralds from sedimentary formations and those of the Gravelotte emeralds from a highly evolved pegmatite. The Muzo sedimentary formations likely had a $(La/Sm)_N$ lower than that the of the Gravelotte pegmatite, due to the relative compatibilities of REE during late stage differentiation, and this feature was transferred to the emerald parental fluids.

The alkali metals, Li, Rb and Cs are strongly enriched in emeralds relative to the bulk CC likely due to the strong affinity of these elements for aqueous fluids parental to emeralds and the presence of fluid inclusions and channels in the beryl structure hosting brines enriched in alkali metals (Grundmann and Morteani, 1989; Ottaway *et al.*, 1994). Concentrations of Rb, Cs and Sr are plotted against Li in **Figure S-4**, showing that the Muzo samples have less Li and Cs (31-43 and 1-4 μg/g, respectively) relative to the Gravelotte samples (292–1590 and 16–234 μg/g, respectively). The Muzo samples plot close to solution ICP-MS analyses of other Colombian emeralds (Alonso-Perez and Day, 2021). However, Gravelotte emeralds are consistently enriched in Li and depleted in Cs and Rb relative to literature data for Gravelotte emeralds indicating that the Gravelotte deposit showed highly heterogeneous alkali element concentrations, or that the two datasets sample significantly different proportions of mineral and fluid inclusions. The deep green color of emerald is attributed to the presence of significant amounts of the chromophoric elements Cr, V and Fe in the beryl lattice (Groat *et al.*, 2008). A normalised ternary diagram of the three chromophores for the samples

and other solution analyses of global emeralds is shown in **Figure S-5**. The new samples, consistent with previous data, show that Colombian emeralds have lower Fe concentrations relative to other global deposits. Gravelotte emeralds plot with other literature data for the deposit and the bulk of other world deposits at the Fe-rich end of the ternary diagram.

Another tool for constraining the origin of emeralds is the abundances of the incompatible element Ga and the compatible elements Ni and Co. While Ga is highly compatible in emeralds (**Figure S-6**), it is a relatively incompatible element during magmatic differentiation, behaving similarly to Al during fractional crystallisation. Gallium is therefore expected to be present in significant quantities in the incompatible element enriched fluids parental to emeralds. In contrast to Ga, both Ni and Co are strongly compatible in olivine, leading to a strong depletion during magmatic differentiation. Therefore, the Ni and Co present in the emeralds from the Gravelotte deposit is likely sourced from the same ultramafic schist that contributed the compatible chromophores Cr and V. The Muzo emeralds, as well as other Colombian emeralds (Alonso-Perez and Day, 2021) show a strong depletion in Ni and Co and a wide range in Ga abundance relative to other global emeralds. This is likely due to the lack of ultramafic lithologies in Colombian emerald deposits (Giuliani *et al.*, 2019) with the emeralds being hosted in organic-rich black shales (Ottaway *et al.*, 1994; Svadlenak, 2015), as shales are not as Ni and Co rich as ultramafic rocks and may also show heterogeneous Ga abundances.

Table S-1 Major element oxide (in wt. %) and trace element (in μg/g) abundances of the studied emeralds as determined by ICP-MS. SiO_2 is determined by difference from the digested weight. Grv- Gravelotte, Mz- Muzo. $FeO_{(t)}$- total iron content expressed as FeO.

Sample	GE-1	GE-2	GE-3a	GE-3b	GE-3c	GE-3d	GE-3e	GE-4	GE-5	GE-6	GE-7	GE-8	97472-1	97472-2
Location	Grv	Grv	Grv	Grv	Grv	Grv	Grv	Grv	Grv	Grv	Grv	Grv	Mz	Mz
SiO_2	71.2	69.1	65.2	61.2	64.7	62.7	68.9	63.2	65.7	78.0	77.2	72.3	78.8	77.4
TiO_2	0.005	0.001	0.003	0.004	0.002	0.004	0.005	0.004	0.005	0.001	0.003	0.005	0.000	0.000
Al_2O_3	9.08	11.2	12.8	14.9	12.6	13.5	8.68	15.7	13.0	4.74	5.42	7.38	6.04	4.70
Cr_2O_3	0.19	0.12	0.08	0.05	0.05	0.05	0.04	0.12	0.28	0.07	0.11	0.27	0.13	0.21
V_2O_5	0.04	0.02	0.04	0.03	0.04	0.04	0.04	0.02	0.04	0.01	0.02	0.03	0.11	0.17
BeO	13.5	13.3	13.8	13.1	14.0	14.2	13.9	13.5	13.9	13.7	13.8	13.8	12.4	14.8
MgO	1.84	2.09	3.02	4.15	2.10	3.31	2.10	2.91	1.34	0.22	0.37	1.52	0.19	0.10
CaO	0.038	0.004	0.022	0.089	0.043	0.056	0.054	0.002	0.016	0.003	0.002	0.012	0.002	0.000
MnO	0.002	0.001	0.002	0.005	0.003	0.004	0.003	0.001	0.003	0.001	0.001	0.001	0.000	0.000
$FeO_{(t)}$	0.48	0.60	0.46	0.53	0.44	0.47	0.44	0.67	0.48	0.16	0.54	0.46	0.42	0.03
Na_2O	1.49	1.45	2.04	2.74	2.76	2.60	2.69	1.64	2.27	1.21	0.94	1.84	0.57	0.96
K_2O	0.035	0.009	0.016	0.035	0.051	0.018	0.067	0.022	0.194	0.006	0.011	0.026	0.002	0.006
P_2O_5	0.000	0.001	0.000	0.001	0.001	0.001	0.002	0.001	0.002	0.000	0.000	0.001	0.000	0.000
H_2O*	2.10	2.07	2.57	3.16	3.18	3.05	3.13	2.24	2.77	1.87	1.64	2.40	1.33	1.66
Li	831	351	1160	1317	1413	1290	1590	368	901	485	292	444	30.8	42.7
B	2.13	1.64	1.71	2.58	2.08	2.01	2.55	0.89	1.99	1.33	1.18	1.61	0.59	0.62
Sc	47.5	14.8	48.0	41.0	40.1	67.0	23.9	20.2	49.7	2.16	2.84	10.8	68.3	30.9
Ti	38.5	10.0	24.4	29.5	24.0	30.2	41.3	27.9	38.4	9.6	22.3	38.1	4.49	5.99
V	189	93.3	203	182	228	214	198	85.7	190	68.0	81.6	159	560	901
Cr	1395	848	547	346	325	333	279	894	1980	515	754	1933	934	1503

Co	1.53	1.46	2.06	2.80	2.27	1.99	2.44	2.09	2.86	1.30	1.08	2.48	0.79	0.006
Ni	19.3	12.3	17.6	27.5	20.2	19.5	23.4	29.2	50.7	15.0	12.8	36.5	4.89	0.71
Cu	3.54	1.26	1.06	1.54	0.89	1.00	1.77	2.43	2.91	2.48	0.69	0.96	1.59	2.67
Zn	11.4	7.35	6.65	9.15	13.3	7.08	53.2	7.51	39.6	4.13	4.45	7.22	2.79	5.65
Ga	15.3	9.71	14.8	14.7	16.5	15.8	15.5	10.3	17.0	13.5	9.59	13.6	38.2	43.2
Ge	0.08	0.18	0.09	0.08	0.06	0.08	0.06	0.18	0.07	0.05	0.11	0.06	0.12	0.02
Rb	8.62	1.99	8.19	11.8	14.1	12.0	12.8	10.4	10.7	0.52	0.83	4.69	0.28	1.98
Sr	1.10	0.26	0.87	3.87	2.73	2.32	3.56	0.37	0.73	0.08	0.09	0.39	0.14	0.16
Y	0.037	0.006	0.044	0.042	0.079	0.128	0.052	0.033	0.021	0.004	0.004	0.006	0.004	0.002
Zr	0.13	0.12	0.83	0.24	0.21	0.31	0.31	0.76	0.23	0.07	0.93	3.57	0.05	0.06
Nb	0.236	0.010	0.098	0.296	0.123	0.145	0.179	0.058	0.659	0.057	0.035	0.259	0.003	0.007
Cs	67.3	34.3	124	103	234	194	194	121	86.5	61.3	15.7	51.7	0.98	3.61
Ba	7.68	0.43	2.17	4.29	2.93	4.09	3.00	2.18	5.96	0.06	0.62	1.44	1.35	0.10
La	0.09	0.030	0.18	0.20	0.10	0.52	0.14	0.020	0.055	0.003	0.082	0.009	0.003	0.003
Ce	0.026	0.046	0.10	0.15	0.22	0.27	0.19	0.007	0.017	0.004	0.17	0.006	0.013	0.005
Pr	0.0222	0.0071	0.0386	0.0400	0.0265	0.1033	0.0288	0.0063	0.0101	0.0008	0.0171	0.0019	0.0008	0.0007
Nd	0.083	0.026	0.133	0.142	0.116	0.347	0.105	0.024	0.040	0.003	0.063	0.006	0.003	0.003
Sm	0.0140	0.0044	0.0197	0.0217	0.0230	0.0509	0.0175	0.0044	0.0066	0.0009	0.0087	0.0014	0.0010	0.0013
Eu	0.0062	0.0009	0.0041	0.0063	0.0051	0.0110	0.0042	0.0019	0.0030	0.0002	0.0013	0.0010	0.0005	0.0002
Gd	0.0113	0.0029	0.0170	0.0177	0.0234	0.0459	0.0162	0.0041	0.0062	0.0007	0.0069	0.0012	0.0009	0.0004
Tb	0.0015	0.0003	0.0019	0.0020	0.0027	0.0048	0.0020	0.0007	0.0009	0.0001	0.0005	0.0001	0.0001	0.0001
Dy	0.0078	0.0010	0.0084	0.0092	0.0142	0.0248	0.0103	0.0047	0.0045	0.0006	0.0014	0.0011	0.0008	0.0005
Ho	0.0014	0.0002	0.0017	0.0016	0.0027	0.0047	0.0018	0.0011	0.0007	0.0001	0.0002	0.0002	0.0002	0.0001
Er	0.0036	0.0006	0.0051	0.0044	0.0070	0.0127	0.0058	0.0039	0.0023	0.0005	0.0004	0.0007	0.0005	0.0002
Tm	0.0006	0.0001	0.0009	0.0006	0.0011	0.0020	0.0010	0.0007	0.0004	0.0001	0.0001	0.0001	0.0001	0.0001
Yb	0.0042	0.0015	0.0100	0.0047	0.0106	0.0169	0.0076	0.0066	0.0039	0.0006	0.0004	0.0013	0.0005	0.0002
Lu	0.0012	0.0004	0.0035	0.0015	0.0033	0.0053	0.0023	0.0016	0.0020	0.0002	0.0001	0.0004	0.0001	0.00004
Hf	0.015	0.007	0.041	0.011	0.017	0.039	0.033	0.031	0.017	0.004	0.037	0.106	0.002	0.002
Ta	0.076	0.002	0.053	0.088	0.043	0.096	0.091	0.007	0.291	0.042	0.009	0.065	0.001	0.002
W	0.43	0.011	0.038	0.12	0.09	0.10	0.14	0.021	0.034	0.025	0.014	0.056	0.005	0.008
Pb	1.06	0.15	1.01	1.46	1.62	1.52	1.81	0.35	0.40	0.08	0.05	0.35	0.51	0.46
Th	0.002	0.005	0.003	0.004	0.003	0.006	0.005	0.003	0.005	0.001	0.001	0.004	0.001	0.001
U	0.004	0.004	0.009	0.011	0.014	0.014	0.026	0.008	0.006	0.005	0.030	0.009	0.003	0.006

Supplementary Figures


(c)
UNITED STATES OF AMERICA
ONE DIME


(d)
UNITED STATES OF AMERICA
ONE DIME


(e)
UNITED STATES OF AMERICA
ONE DIME

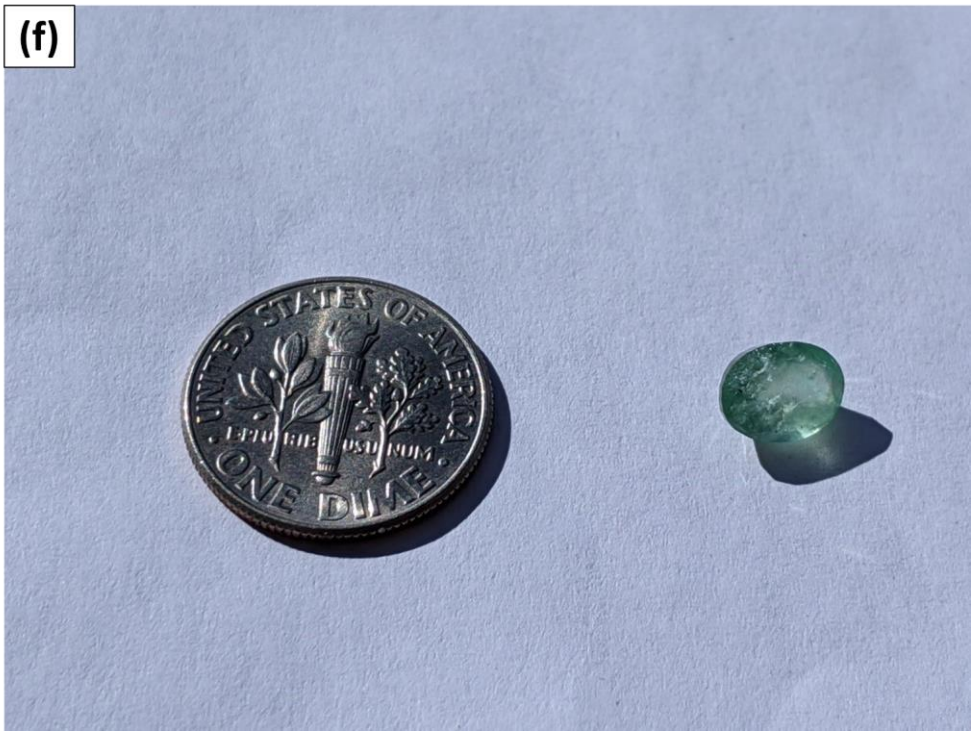
(f)
UNITED STATES OF AMERICA
ONE DIME


(g)
UNITED STATES OF AMERICA
ONE DIME


(h)
UNITED STATES OF AMERICA
ONE DIME

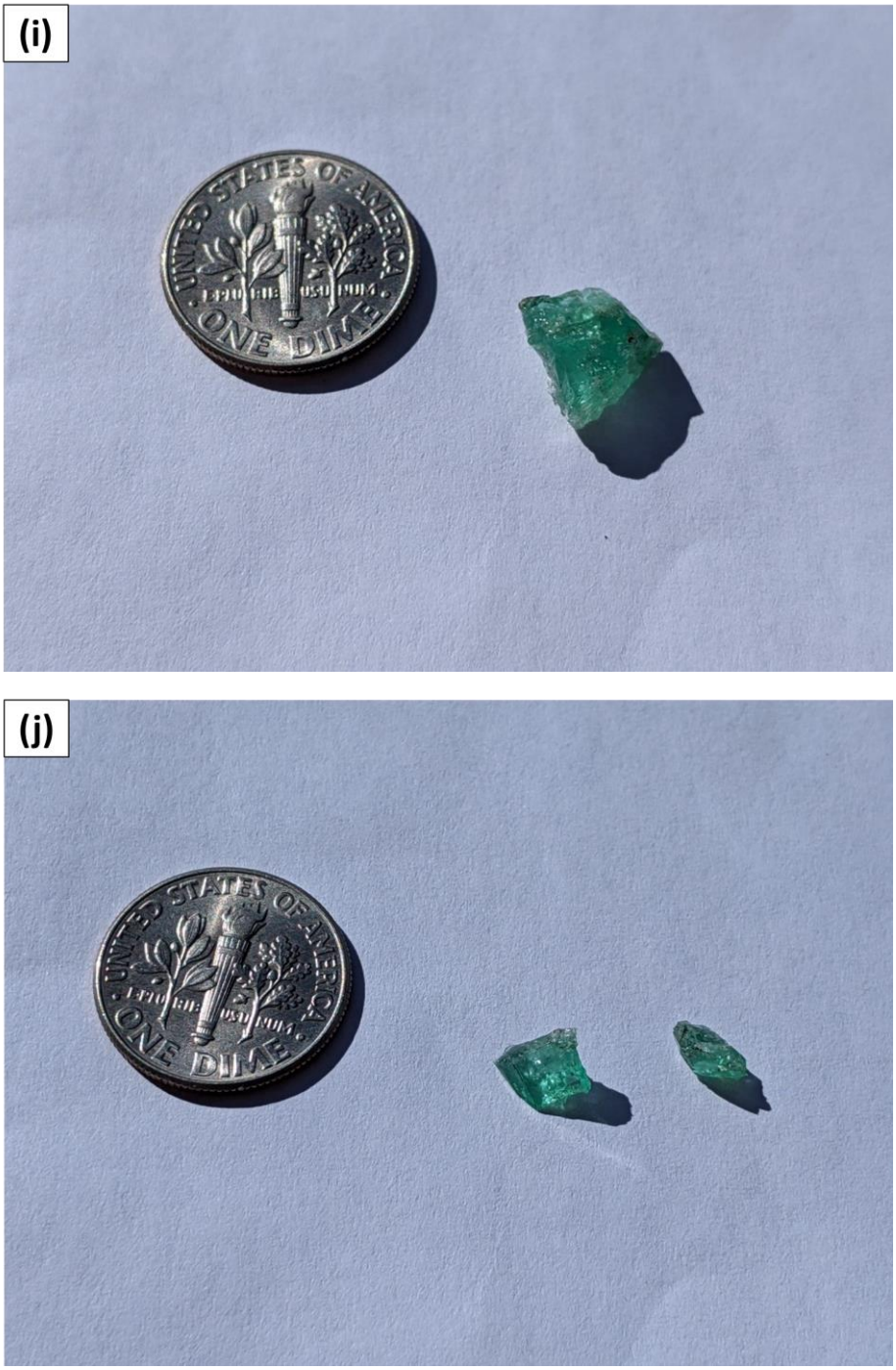

Figure S-1 **(a)** Photograph of sample GE-1. **(b)** Photograph of sample GE-2. **(c)** Photograph of sample GE-3. **(d)** Photograph of sample GE-4. **(e)** Photograph of sample GE-5. **(f)** Photograph of sample GE-6. **(g)** Photograph of sample GE-7. **(h)** Photograph of sample GE-8. **(i)** Photograph of sample 97472-1. **(j)** Photograph of sample 97472-2.

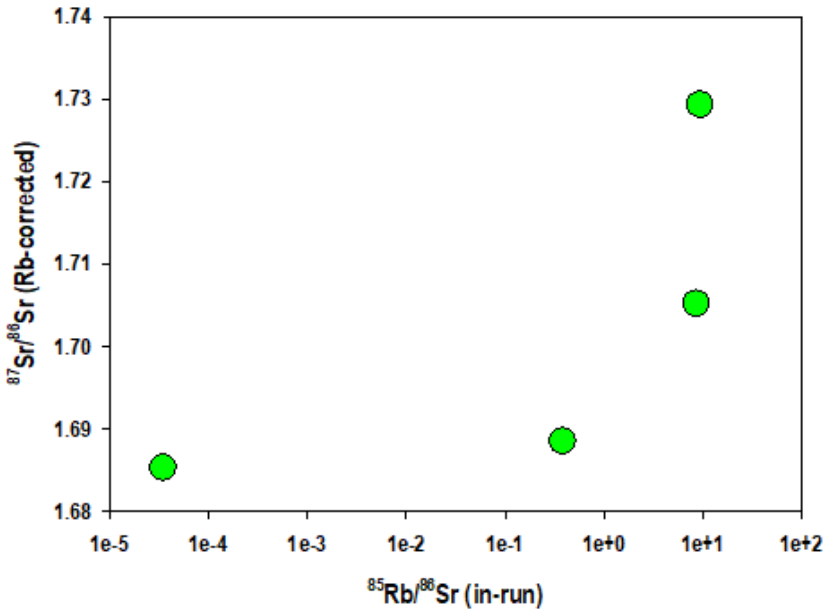

Figure S-2 Evaluation of the validity of the ^{87}Rb interference correction on the reported $^{87}Sr/^{86}Sr$ ratios. For some, but not all samples, the high Rb/Sr and low Sr contents led to some residual Rb on the loaded filament after column chemistry. Plotted are four sequential runs of the same filament of sample GE-4a, showing how Rb was exhausted from the filament during each run. The first run was the right most, with repeat runs showing progressively lower in-run Rb/Sr. Interference correction was made using the $^{85}Rb/^{86}Sr$ ratio assuming an unfractionated $^{87}Rb/^{85}Rb$ ratio of 0.386. The final two runs of the filament, with $^{85}Rb/^{86}Sr$ ratios of 0.387 and 0.000035, respectively yield interference corrected $^{87}Sr/^{86}Sr$ ratios within 0.0032 of each other. This indicates that even high $^{85}Rb/^{86}Sr$ ratios of 0.387 do not have a strong effect on the data reported, or the conclusions of this paper. All reported data in **Table 1** show in-run $^{85}Rb/^{86}Sr$ ratios <0.062, with the majority below 0.005, demonstrating that correction for ^{87}Rb interference is not the cause of the spread in measured $^{87}Sr/^{86}Sr$ ratios.

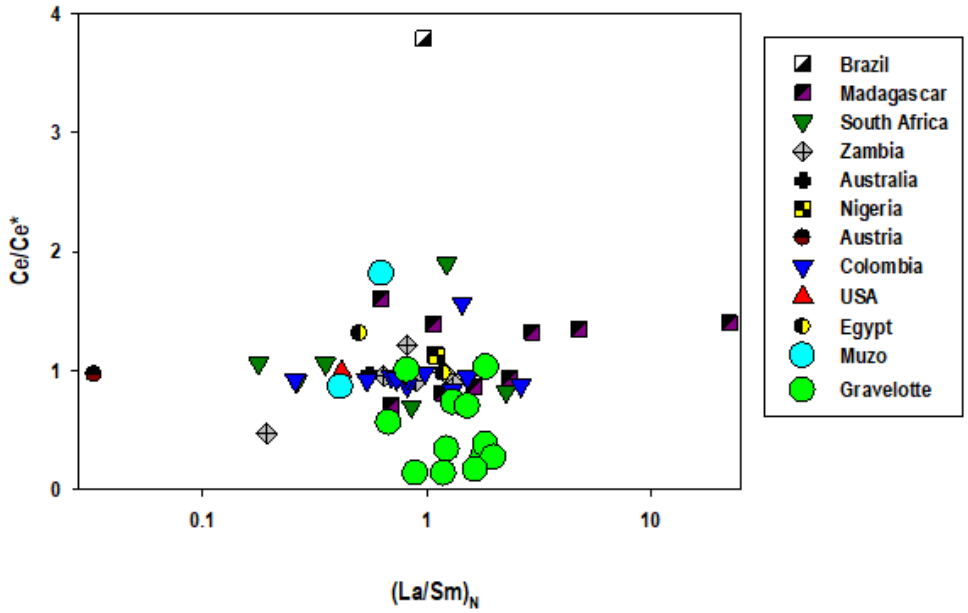

Figure S-3 Continental crust (UCC) normalised $(La/Sm)_N$ ratios plotted against Ce anomalies ($Ce/Ce^* = Ce_N/(La_N*Pr_N)^{0.5}$) of complete dissolutions of emeralds from global deposits. Normalising values for continental crust are from Rudnick and Gao (2014); the emerald bulk solution data other than for Muzo and Gravelotte are from Alonso-Perez and Day (2021).

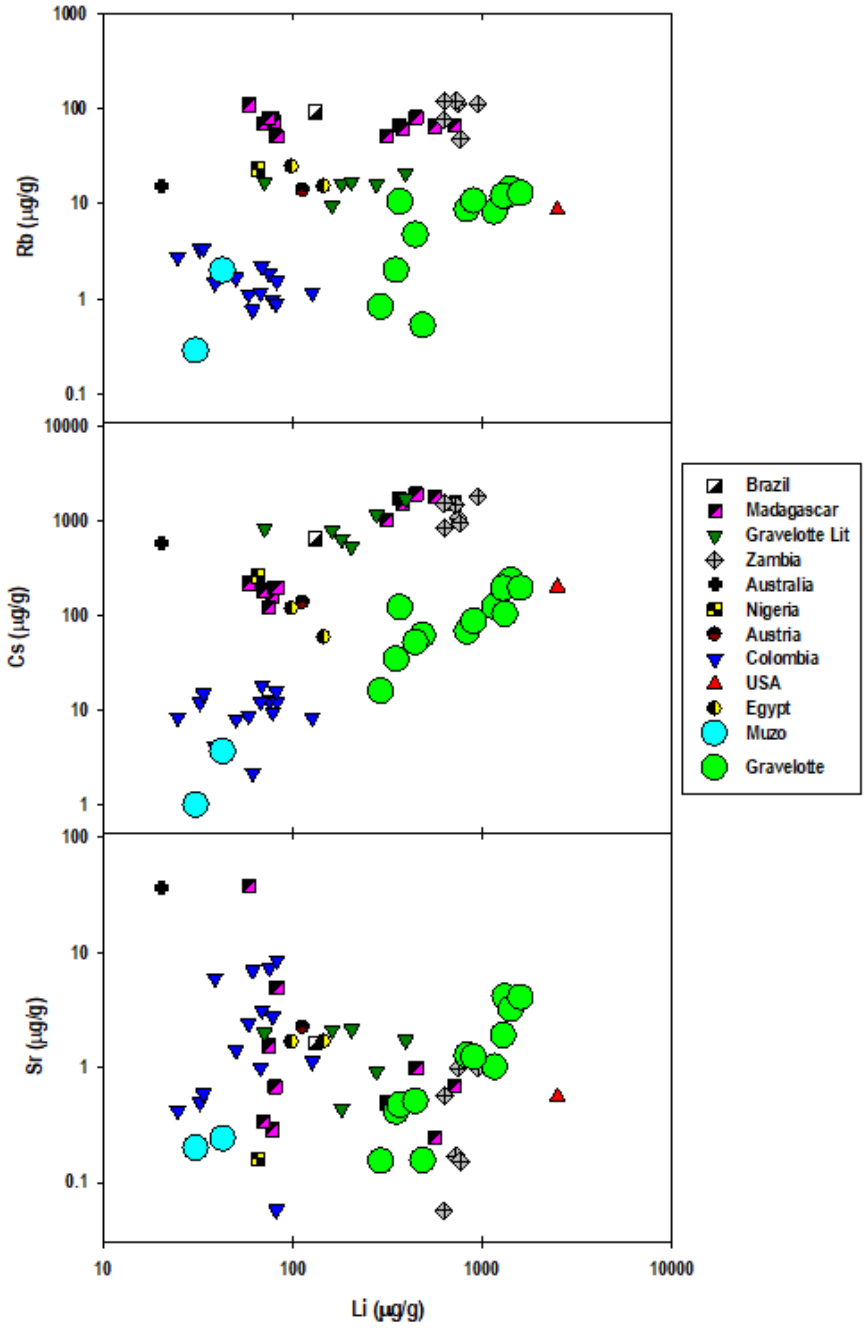

Figure S-4 Abundances of Li (in µg/g) plotted against Rb (in µg/g), Cs and Sr abundances (in µg/g) for global emeralds. Literature data taken from Alonso-Perez and Day (2021).

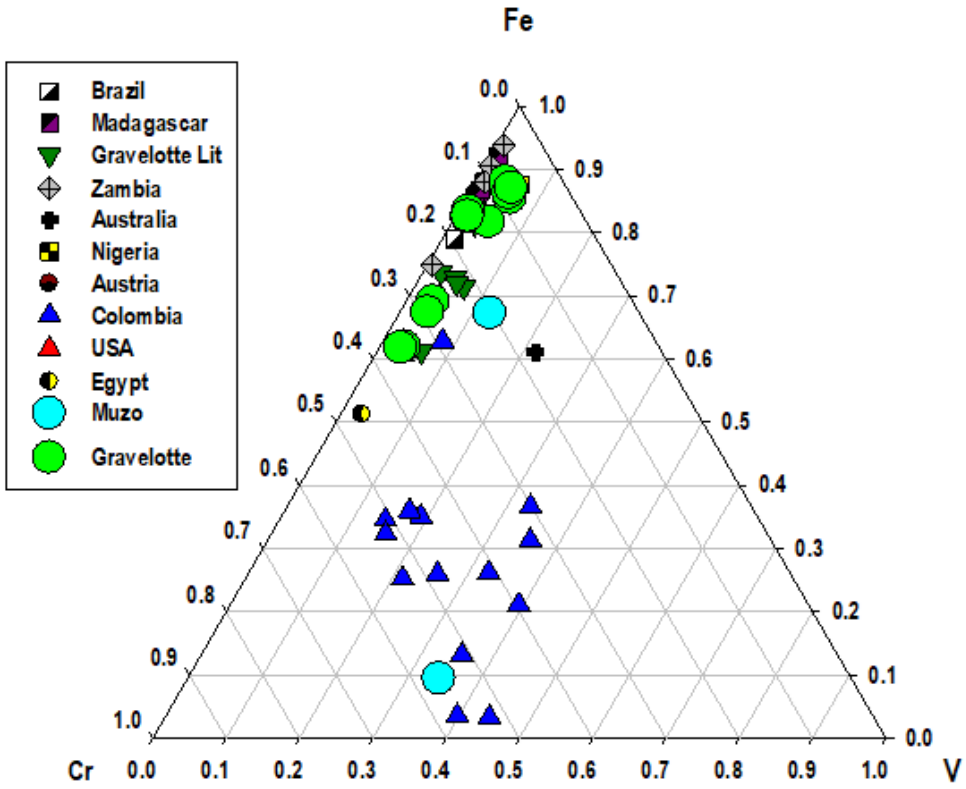

Figure S-5 Ternary diagram showing normalised molar abundances of the chromophores V, Fe and Cr in global emeralds. Literature data taken from Alonso-Perez and Day (2021).

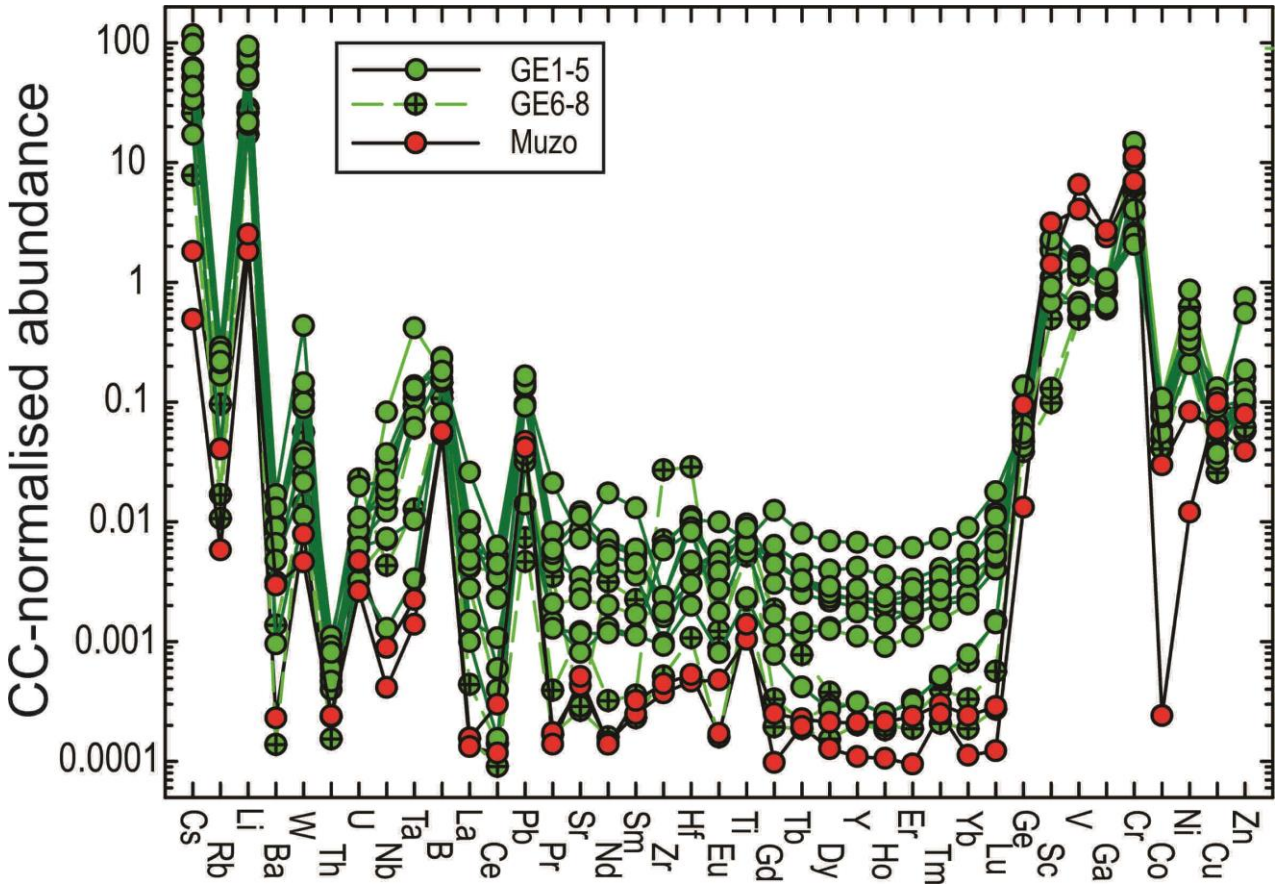

Figure S-6 Abundances of trace elements in the studied emeralds ordered according to incompatibility during mantle melting, normalised to the bulk CC (Rudnick and Gao, 2014).

Supplementary Information References

Alonso-Perez, R., Day, J.M.D. (2021) Rare earth element and incompatible trace element abundances in emeralds reveal their formation environments. *Minerals* 11, 1–21. https://doi.org/10.3390/min11050513

Banks, D. A., Giuliani, G., Yardley, B.W.D., Cheilletz, A. (2000) Emerald mineralisation in Colombia: fluid chemistry and the role of brine mixing. *Mineralium Deposita* 35, 699-713. https://doi.org/10.1007/s001260050273

Byrne, R.H., Sholkovitz, E.R. (1996) Chapter 158: Marine chemistry and geochemistry of the lanthanides. *Handbook on the Physics and Chemistry of Rare Earths* 23, 497–593. https://doi.org/10.1016/S0168-1273(96)23009-0

Cheilletz, A., Feraud, G., Giuliani, G., Ruffet, G. (1993) Emerald dating through $^{40}Ar/^{39}Ar$ step-heating and laser spot analysis of syngenetic phlogopite. *Earth and Planetary Science Letters* 120, 473–485. https://doi.org/10.1016/0012-821X(93)90258-B

Dereppe, J.M., Moreaux, C., Chauvaux, B., Schwarz, D. (2000) Classification of emeralds by artificial neural networks. *Journal of Gemology* 27, 2, 93–105. https://doi.org/10.15506/JoG.2000.27.2.93

Giuliani, G., France-Lanord, C., Zimmermann, J.L., Cheilletz, A., Arboleda, C., Charoy, B., Coget, P., Fontan, F., Giard, D. (1997) Fluid composition, δD of channel H_2O, and $\delta^{18}O$ of lattice oxygen in beryls: genetic implications for Brazilian, Colombian, and Afghanistani emerald deposits. *International Geology Review* 39, 400–424. https://doi.org/10.1080/00206819709465280

Giuliani, G., Groat, L.A., Marshall, D., Fallick, A.E., Branquet, Y. (2019) Emerald Deposits: A Review and Enhanced Classification. *Minerals*, 105, 1–63. https://doi.org/10.3390/min9020105

Giuliani, G., France-Lanord, C., Cheilletz, A., Coget, P., Branquet, Y., Laumomnier, B. (2000) Sulfate Reduction by Organic Matter in Colombian Emerald Deposits: Chemical and Stable Isotope (C, O, H) Evidence. *Economic Geology* 95, 1129–1153. https://doi.org/10.2113/gsecongeo.95.5.1129

Groat, L.A., Marshall, D.D., Giuliani, G., Murphy, D.C., Piercey, S.J., Jambor, J.L., Mortensen, J.K., Ercit, T.S., Gault, R.A., Mattey, D.P., Schwarz, D., Maluski, H., Wise, M.A., Wengzynowski, W., Eaton, D.W. (2002) Mineralogical and Geochemical Study of the Regal Ridge Emerald Showing, Southeastern Yukon. *The Canadian Mineralogist* 40, 1313–1338. https://doi.org/10.2113/gscanmin.40.5.1313

Grew, E.S., Hazen, R.M. (2014) Beryllium mineral evolution. *American Mineralogist* 99, 999–1021. https://doi.org/10.2138/am.2014.4675

Grundmann, G., Morteani, G. (1989) Emerald Mineralization during Regional Metamorphism: The Habachtal (Austria) and Leydsdorp (Transvaal, South Africa) Deposits. *Economic Geology* 84, 835–1849. https://doi.org/10.2113/gsecongeo.84.7.1835

Lum, J.E., Viljoen, K.S., Cairncross, B. (2016) Mineralogical and geochemical characteristics of emeralds from the Leydsdorp area, South Africa. *South African Journal of Geology* 119, 2, 359–378. https://doi.org/10.2113/gssajg.119.2.359

Lyons, T.W., Reinhard, C.T., Planavsky, N.J. (2014) The rise of oxygen in Earth's early ocean and atmosphere. *Nature* 506, 307–315. https://doi.org/10.1038/nature13068

Nwe, Y.Y., Morteani, G. (1993) Fluid evolution in the H_2O-CH_4-CO_2-NaCl system during emerald mineralization at Gravelotte, Murchison Greenstone Belt, Northeast Transvaal, South Africa. *Geochimica et Cosmochimica Acta* 57, 89–103. https://doi.org/10.1016/0016-7037(93)90471-8

Ottaway, T.L., Wicks, F.J., Bryndzia, L.T., Kyser, T.K., Spooner E.T.C. (1994) Formation of the Muzo hydrothermal emerald deposit in Colombia. *Nature* 369, 552–554. https://doi.org/10.1038/369552a0

Poujol, M. (2001) U-Pb isotopic evidence for episodic granitoid emplacement in the Murchison greenstone belt, South Africa. *Journal of African Earth Sciences* 33, 155–163. https://doi.org/10.1016/S0899-5362(01)90096-X

Rainer T., Davidson P., Rericha A. (2020) Emerald from the Habachtal: new observations. *Mineralogy and Petrology* 141, 161–173. https://doi.org/10.1007/s00710-020-00700-4

Robb, L.J., Robb, V.M. (1986) Archean pegmatite deposits in the northeastern Transvaal. In: Anhaeusser, C.R., Maske, S. (Eds.) *Mineral Deposits of Southern Africa: Geological Society of South Africa*. Geological Society of South Africa, Johannesburg, South Africa, 437–450.

Rudnick, R.L., Gao, S. (2014) 4.1 - Composition of the Continental Crust. In: Holland, H.D., Turkenian, K.K. (Eds.) *Treatise on Geochemistry*. 2nd edition, Elsevier, Amsterdam, 1–51. https://doi.org/10.1016/B978-0-08-095975-7.00301-6

Saeseaw, S., Renfro, N.D., Palke, A.C., Sun, Z., McClure, S.F. (2020) Geographic origin determination of Emerald. *Gems and Gemology* 55, 614–646. https://doi.org/10.5741/GEMS.55.4.614

Svadlenak, E. (2015) $^{40}Ar/^{39}Ar$ Ages and Trace Element Variations in Colombian Emeralds. [Honors Baccalaureate Thesis], Corvallis, Oregon State University.

Thomas, R., Davidson, P., Rericha, A. (2020) Emerald from the Habachtal: new observations. *Mineralogy and Petrology* 114, 161–173. https://doi.org/10.1007/s00710-020-00700-4